

# Global phytoplankton decline over the past century

Daniel G. Boyce<sup>1</sup>, Marlon R. Lewis<sup>2</sup> & Boris Worm<sup>1</sup>

**In the oceans, ubiquitous microscopic phototrophs (phytoplankton) account for approximately half the production of organic matter on Earth. Analyses of satellite-derived phytoplankton concentration (available since 1979) have suggested decadal-scale fluctuations linked to climate forcing, but the length of this record is insufficient to resolve longer-term trends. Here we combine available ocean transparency measurements and *in situ* chlorophyll observations to estimate the time dependence of phytoplankton biomass at local, regional and global scales since 1899. We observe declines in eight out of ten ocean regions, and estimate a global rate of decline of ~1% of the global median per year. Our analyses further reveal interannual to decadal phytoplankton fluctuations superimposed on long-term trends. These fluctuations are strongly correlated with basin-scale climate indices, whereas long-term declining trends are related to increasing sea surface temperatures. We conclude that global phytoplankton concentration has declined over the past century; this decline will need to be considered in future studies of marine ecosystems, geochemical cycling, ocean circulation and fisheries.**

Generating roughly half the planetary primary production<sup>1</sup>, marine phytoplankton affect the abundance and diversity of marine organisms, drive marine ecosystem functioning, and set the upper limits to fishery yields<sup>2</sup>. Phytoplankton strongly influence climate processes<sup>3</sup> and biogeochemical cycles<sup>4,5</sup>, particularly the carbon cycle. Despite this far-reaching importance, empirical estimates of long-term trends in phytoplankton abundance remain limited.

Estimated changes in marine phytoplankton using satellite remote sensing (1979–86 and 1997–present) have been variable<sup>6</sup>, with reported global decreases<sup>7</sup> and increases<sup>8,9</sup>, and large interannual<sup>10</sup> and decadal-scale variability<sup>11</sup>. Despite differences in scale and approach, it is clear that long-term estimates of phytoplankton abundance are a necessary, but elusive, prerequisite to understanding macroecological changes in the ocean<sup>10–13</sup>.

Phytoplankton biomass is commonly inferred from measures of total chlorophyll pigment concentration ('Chl'). As Chl explains much of the variance in marine primary production<sup>14</sup> and captures first-order changes in phytoplankton biomass, it is considered a reliable indicator of both phytoplankton production and biomass<sup>15</sup>. Shipboard measurements of upper ocean Chl have been made since the early 1900s, first using spectrophotometric and then fluorometric analyses of filtered seawater residues, and more recently through *in vivo* measurements of phytoplankton fluorescence<sup>16</sup>. Additionally, measurements of upper ocean transparency using the standardized Secchi disk are available from 1899 to present and can be related to surface Chl through empirically based optical equations<sup>17,18</sup>. Although the Secchi disk is one of the oldest and simplest oceanographic instruments, Chl concentrations derived from Secchi depth observations are closely comparable to those estimated from direct *in situ* optical measurements or satellite remote sensing<sup>18</sup>.

We compiled publicly available *in situ* Chl and ocean transparency measurements collected in the upper ocean over the past century (Fig. 1a–c; see Supplementary Information for data sources). Transparency measurements were converted to depth-averaged Chl concentrations using established models<sup>17</sup>. Systematic filtration algorithms were applied to remove erroneous and biologically unrealistic Chl measurements, and to exclude those in waters <25 m deep or

<1 km from the coast, where terrigenous and re-suspended substances introduce optical errors. *In situ* and transparency derived Chl measurements (monthly averages for each year, 0.25° resolution) were strongly correlated ( $r = 0.52$ ;  $P < 0.0001$ ). After log-transforming these data to achieve normality and homoscedasticity, model II major axis regression analysis revealed linear scaling of transparency-derived and *in situ*-derived Chl (intercept, 0.18; slope,  $1.08 \pm 0.016$ ;  $r^2 = 0.60$ ). Both this and additional analyses indicated that both data sources were statistically similar enough to combine (see Methods and Supplementary Figs 2, 3). The blended data consisted of 445,237 globally distributed Chl measurements collected between 1899 and 2008 (Fig. 1a). Data density was greatest in the North Atlantic and Pacific oceans and after 1930 (Fig. 1b, c), and broadly reproduced spatial patterns of phytoplankton biomass derived from remote sensing<sup>7</sup> (Fig. 1d and Supplementary Fig. 3).

Chl trends were estimated using generalized additive models (GAMs)<sup>19</sup>. These models are extensions of generalized linear models that do not require prior knowledge of the shape of the response function. To ensure robustness, Chl trends were estimated at three different spatial scales—local, regional and global.

## Local-scale phytoplankton trends

To estimate local Chl trends, blended data were binned onto a 10° × 10° global grid and GAMs of Chl as log-linear functions of covariates were fitted to data within each cell. Phytoplankton declines were observed in 59% ( $n = 214$ ) of the cells containing sufficient data (Fig. 2a, b). Clusters of increasing cells were found across the eastern Pacific, and the northern and eastern Indian Ocean (Fig. 2b). High-latitude areas (>60°) showed the greatest proportion of declining cells (range: 78–80%).

Owing to sparse observations in early years, local trends were also estimated using post-1950 data only. This yielded almost identical results, although the magnitude of change was amplified in some cells (see Supplementary Fig. 7).

Local models further suggested that Chl has declined more rapidly with increasing distance from land (Fig. 2c). This agrees with results derived from satellite data, documenting declining phytoplankton in

<sup>1</sup>Biology Department, Dalhousie University, Halifax, Nova Scotia, Canada, B3H 4J1. <sup>2</sup>Department of Oceanography, Dalhousie University, Halifax, Nova Scotia, Canada, B3H 4J1.

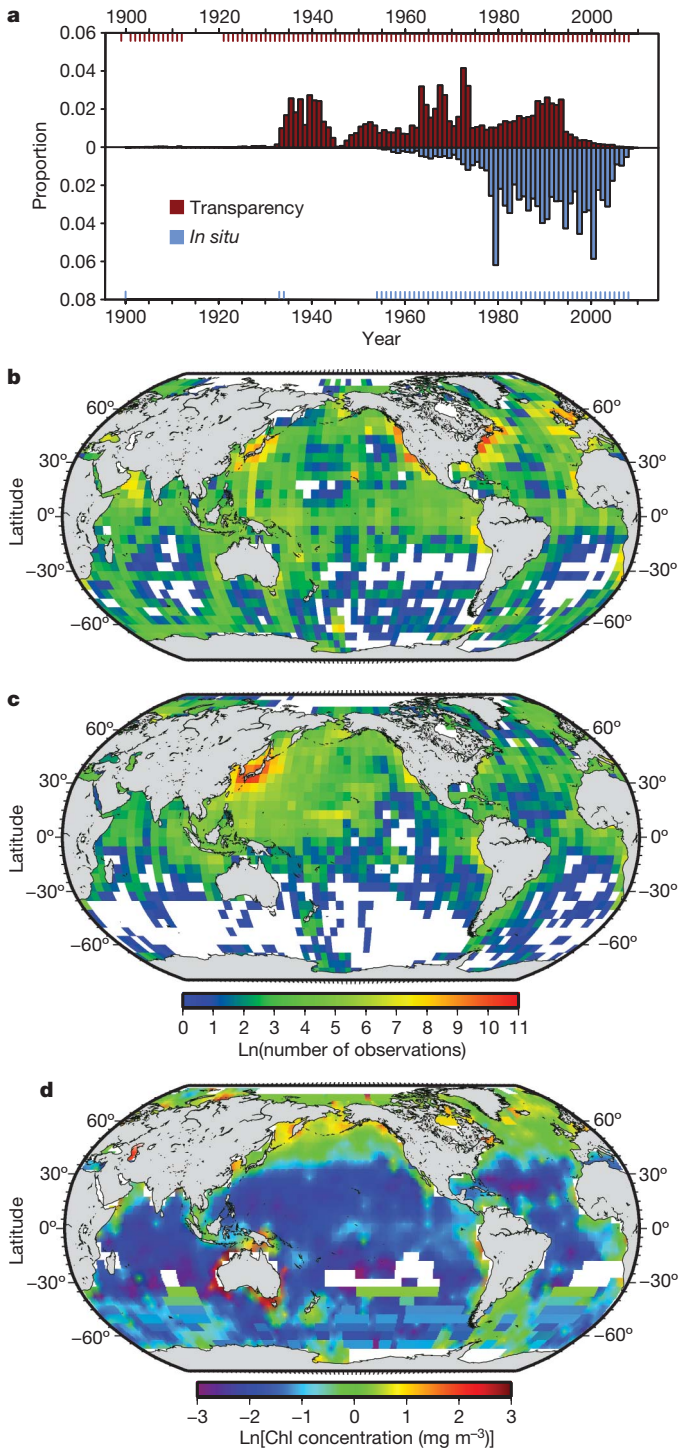


**Figure 1 | Data availability.** **a**, Temporal availability of ocean transparency (red), and *in situ* Chl (blue) measurements. Bars represent the proportion of total observations collected in each year, coloured ticks on x axes represent years containing data. **b**, **c**, Spatial distribution of *in situ* Chl (**b**) and transparency data (**c**). Colours depict the number of measurements per  $5^\circ \times 5^\circ$  cell (ln-transformed). **d**, Averaged Chl concentration from blended transparency and *in situ* data per cell.

the open oceans<sup>8,20,21</sup>, and expansion of oligotrophic gyres, probably due to intensifying vertical stratification and ocean warming<sup>10,22</sup>. These trends are noteworthy, because most (75%) aquatic primary production occurs in these waters<sup>23</sup>. In shelf regions, Chl trends switched from negative to positive in more recent years (since ~1980), consistent with reported Chl increases due to intensifying coastal eutrophication and land runoff<sup>8</sup>.

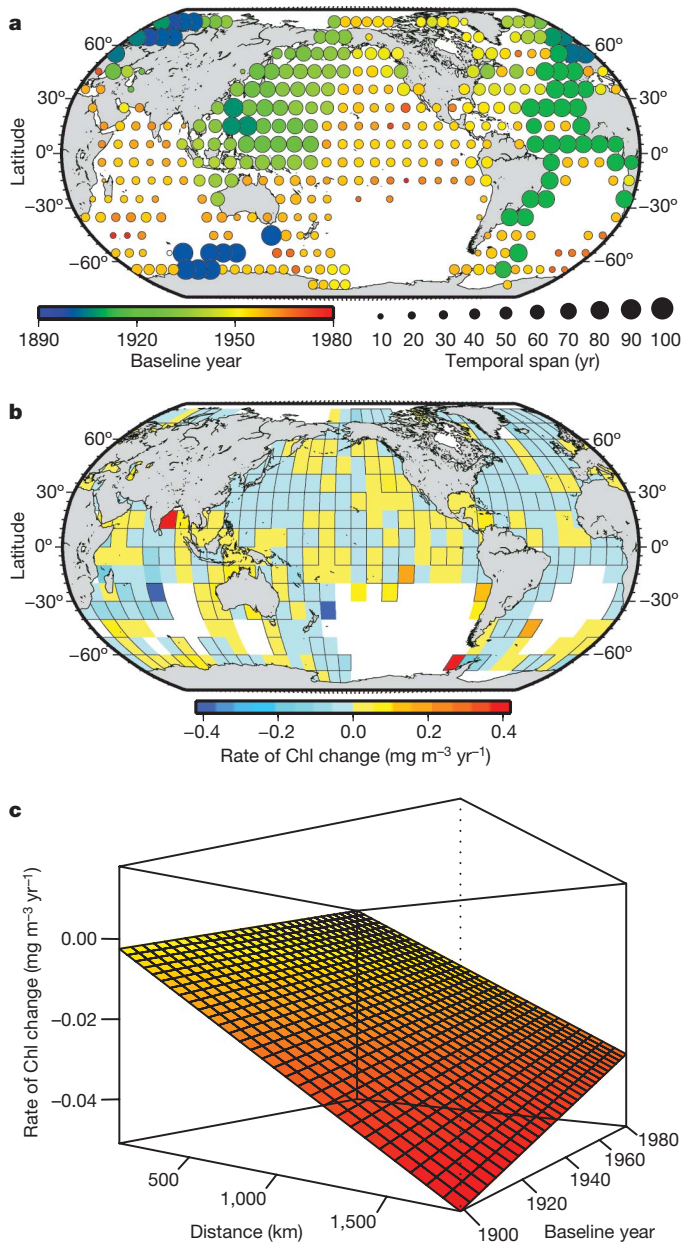


**Figure 2 | Local-scale trends in phytoplankton.** **a**, Baseline year and temporal span of Chl data used in local models. **b**, Mean instantaneous rates of Chl change in each  $10^\circ \times 10^\circ$  cell ( $n = 364$ ). Yellow and red represent cells where Chl has increased, while blue represents a Chl decrease. Cells bordered in black denote statistically significant rates of change ( $P < 0.05$ ) and white cells indicate insufficient data. **c**, Mean instantaneous rates of Chl change for each  $10^\circ \times 10^\circ$  cell, estimated as a function of distance from the nearest coastline (km) and baseline year of trend. Colour shading depicts the magnitude of change per year. All effects used to fit the trend surface were statistically significant ( $P < 0.05$ ).

### Regional and global phytoplankton trends

To estimate regional Chl trends, we divided the global ocean into ten regions, in which similar variability in phytoplankton biomass was observed in response to seasonality and climate forcing<sup>24</sup> (Fig. 3a). To capture the range of potential Chl trajectories, regional trends were estimated from GAMs as linear functions of time on a log scale in three different ways: (1) continuous (linear trend), (2) discrete (mean year-by-year estimates), and (3) smooth functions of time (non-monotonic trend). This approach is comprehensive; it allows both the quantitative (magnitude) and qualitative nature (shape) of trends to be estimated (see Methods Summary and Supplementary Information for full details).

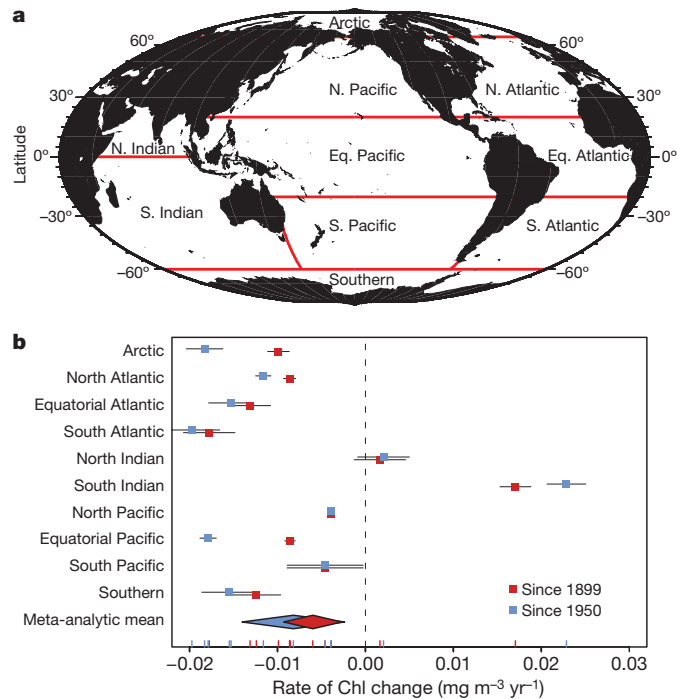


**Figure 3 | Regional and global trends in phytoplankton.** **a**, Ocean regions ( $n = 10$ ) used to estimate regional trends in Chl. N., North; Eq., Equatorial; S., South. **b**, Mean instantaneous rates of Chl change estimated for each region, with 95% confidence limits. Diamonds indicate the global meta-analytic mean rate of Chl change, with 95% confidence intervals. Trends were estimated using all available data (red symbols) and data since 1950 only (blue symbols). Individual estimates are displayed as tick-marks on the  $x$  axis. All estimates were statistically significant ( $P < 0.05$ ), except for the North Indian region ( $P = 0.27$ ).

Estimation of Chl trends as continuous log-linear functions of time revealed phytoplankton declines in eight out of the ten regions. The largest rates of decline were observed in the South Atlantic ( $-0.018 \pm 0.0015 \text{ mg m}^{-3} \text{ yr}^{-1}$ ), Southern ( $-0.015 \pm 0.0016 \text{ mg m}^{-3} \text{ yr}^{-1}$ ), and Equatorial Atlantic ( $-0.013 \pm 0.0012 \text{ mg m}^{-3} \text{ yr}^{-1}$ ) regions ( $P < 0.0001$  for all trends; Fig. 3b). Increases were observed in the North Indian ( $0.0018 \pm 0.0015 \text{ mg m}^{-3} \text{ yr}^{-1}$ ;  $P = 0.268$ ) and South Indian regions ( $0.02 \pm 0.0011 \text{ mg m}^{-3} \text{ yr}^{-1}$ ;  $P < 0.0001$ ). The global meta-analytic mean rate of Chl change derived from individual regional model estimates was  $-0.006 \pm 0.0017 \text{ mg m}^{-3} \text{ yr}^{-1}$  ( $P < 0.0001$ ; Fig. 3b), representing an annual rate of decline of  $\sim 1\%$  relative to the global median chlorophyll concentration ( $\sim 0.56 \text{ mg m}^{-3}$ ).

Regional trends were also estimated using data since 1950 only, but the direction of all trends remained unchanged and the magnitude of changes was minimal (Fig. 3b). Post-1950 trends were amplified in some regions, resulting in a greater but more variable global rate of decline ( $-0.008 \pm 0.0068 \text{ mg m}^{-3} \text{ yr}^{-1}$ ;  $P < 0.0001$ ). Estimating regional trends separately for each data source yielded similar results (see Supplementary Fig. 4).

Modelling Chl trends as both discrete and smooth functions of time revealed pronounced interannual to decadal fluctuations superimposed on long-term trends (Fig. 4a). We observed greater Chl fluctuations in the Southern Hemisphere regions and greater uncertainty about estimates before 1950; both issues probably reflect limitations in data availability for these regions and time periods. In the polar and Atlantic regions, Chl increased until  $\sim 1950$ , before undergoing prolonged declines (about 1950–95). After  $\sim 1995$ , sharp increases were observed in the South Indian and Southern regions (Fig. 4a).

GAMs also accounted for mean seasonal variation in Chl (Fig. 4b) and closely reproduced known patterns<sup>24,25</sup>, providing a measure of confidence in our approach. Strong seasonality in polar regions

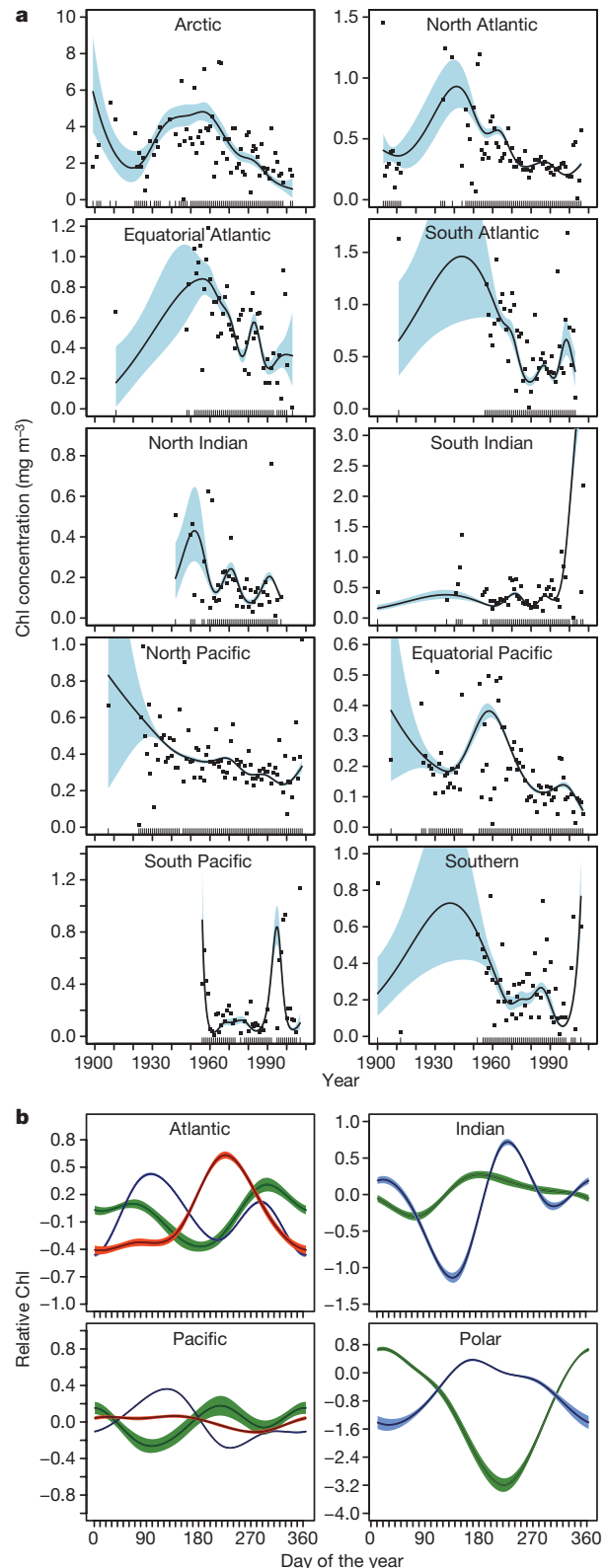


**Figure 4 | Temporal variability in phytoplankton trends.** **a**, GAM estimates of Chl as a discrete (points) or smooth function (lines) of yearly variability in each region ( $n = 10$ ). For each initial year, Chl is the arithmetic, rather than model-estimated, mean. Temporal data availability is displayed as tick-marks on the  $x$  axis. **b**, Seasonal patterns of Chl as a smooth function of day of year in each northern (blue), equatorial (red) and southern (green) ocean. Shaded areas represent approximate 95% Bayesian credible limits around each estimate.



reflects pronounced variability in mixing, irradiance and ice cover<sup>26</sup> whereas weak seasonality in equatorial regions is a function of near-constant solar irradiance. Complex seasonality in the Indian Ocean relates to the effects of monsoon dynamics and freshwater inputs on nutrient delivery<sup>27</sup>. Temperate regions are affected by seasonally changing solar irradiance and trade winds, and their effects on upper ocean nutrient delivery<sup>28</sup>.

### Climate effects on phytoplankton

Regional phytoplankton trends display both short-term variation and longer-term trends. We tested the hypothesis that the short-term (interannual to decadal) component in Chl variation may be explained by the effects of leading climate oscillators, such as the El Niño/Southern Oscillation (ENSO) or the North Atlantic Oscillation (NAO). After de-trending and removing seasonal variation, yearly Chl anomalies were strongly negatively correlated with the bivariate ENSO index in the Equatorial Pacific ( $r = -0.45$ ;  $P < 0.0001$ ; Fig. 5a). Positive ENSO phases are associated with warming sea surface temperatures (SSTs), increased stratification, and a deeper nutrient-cline, leading to negative Chl anomalies in the Equatorial Pacific<sup>10,11</sup>. Negative correlations were also found between the NAO index and

Chl in the North Atlantic ( $r = -0.31$ ;  $P = 0.0002$ ; Fig. 5b) and Equatorial Atlantic ( $r = -0.44$ ;  $P = 0.001$ ) regions, in accordance with results from Continuous Plankton Recorder surveys<sup>29</sup>. Positive NAO phases are associated with intensifying westerly winds and warmer SST in Europe and the central North Atlantic<sup>30</sup>. Possibly, the observed effects relate to increased westerly wind intensity during the winter months, when annual phytoplankton productivity is limited by light availability associated with deep mixed layer depths (MLD)<sup>29</sup>. We put forward a hypothesis: that an observed coupling of NAO and wind intensity to regional zooplankton abundances<sup>29,30</sup> represents a trophic response to the observed phytoplankton fluctuations.

No significant relationship was found between the Indian Ocean Dipole index and Chl in the North Indian region ( $r = -0.23$ ;  $P = 0.18$ ). The Atlantic Multidecadal Oscillation was positively correlated with Chl in all Atlantic regions (range:  $r = 0.31$ – $0.43$ ;  $P < 0.05$  for all). Chl anomalies in the Arctic region were negatively correlated with the Arctic Oscillation index ( $r = -0.31$ ;  $P = 0.01$ ; Fig. 5c). Chl anomalies in the Southern region were negatively correlated with the Antarctic Oscillation index ( $r = -0.48$ ;  $P = 0.029$ ; Fig. 5d), again, possibly owing to intensifying westerly winds and deep MLDs. The strength of all relationships increased after 1950, indicating that phytoplankton may be increasingly driven by climate variability or, alternatively, that model accuracy increased because of increased data availability.

### Physical drivers of phytoplankton trends

Long-term trends in phytoplankton could be linked to changes in vertical stratification and upwelling<sup>10,11,22</sup>, aerosol deposition<sup>31</sup>, ice, wind and cloud formation<sup>8,32</sup>, coastal runoff<sup>20</sup>, ocean circulation<sup>33</sup> or trophic effects<sup>34</sup>. For parsimony, we focus on three variables that may reflect the coupling between physical climate variability and the Chl concentration in the upper ocean: ocean MLD (1955–2009), wind intensity at 10 m (1958–2009) and SST (1899–2009). These physical variables (monthly averages, 1° resolution) were matched by time (year, month) and location (1° cell) with Chl data in order to estimate their effects on Chl within a single model framework (see Supplementary Information for details). SST was the strongest single predictor of Chl. Rising SSTs over most of the global ocean (Fig. 6a) were associated with declining Chl in eight out of the ten regions (range:  $-0.21$  to  $-0.019 \text{ mg m}^{-3} \text{ } ^\circ\text{C}^{-1}$ ;  $P < 0.0001$  for all). Positive relationships between SST and Chl were found in the Arctic ( $0.067 \text{ mg m}^{-3} \text{ } ^\circ\text{C}^{-1}$ ;  $P < 0.0001$ ) and Southern regions ( $0.002 \text{ mg m}^{-3} \text{ } ^\circ\text{C}^{-1}$ ;  $P = 0.11$ ). Likewise, inclusion of SST as a covariate in our local models revealed negative SST effects on Chl in 76% ( $n = 118$ ) of  $10^\circ \times 10^\circ$  cells (Fig. 6b). Negative effects prevailed at low latitudes and strong positive effects at high latitudes, particularly in the Southern Ocean ( $P < 0.05$  for all; Fig. 6b and c).

The effects of SST on Chl are probably explained by its influence on water column stability and MLD<sup>10,22</sup>. Increasing SST leads to a shallower mixed layer, which further limits nutrient supply to phytoplankton in already stratified tropical waters, but may benefit phytoplankton at higher latitudes where growth is constrained by light availability and deep mixing<sup>35</sup>. Indeed, in our local models MLD was a significant, but weaker, predictor of Chl concentrations compared with SST, possibly owing to the reduced time series span (1955–2009). Latitudinal gradients in MLD effects were also observed, with predicted positive effects between 20° N and 20° S and negative effects in polar areas ( $r^2 = 0.1$ ;  $P = 0.018$ ; Fig. 6d). Cumulatively, these findings suggest that warming SST and reduced MLD may be responsible for phytoplankton declines at low latitudes. This mechanism, however, does not explain observed phytoplankton declines in polar areas, where ocean warming would be predicted to enhance Chl (Fig. 6c). This may partially be explained by concurrent increases in MLD and wind intensity there (see Supplementary Fig. 9). Further work is needed to understand the complex oceanographic drivers of phytoplankton trends in polar waters.

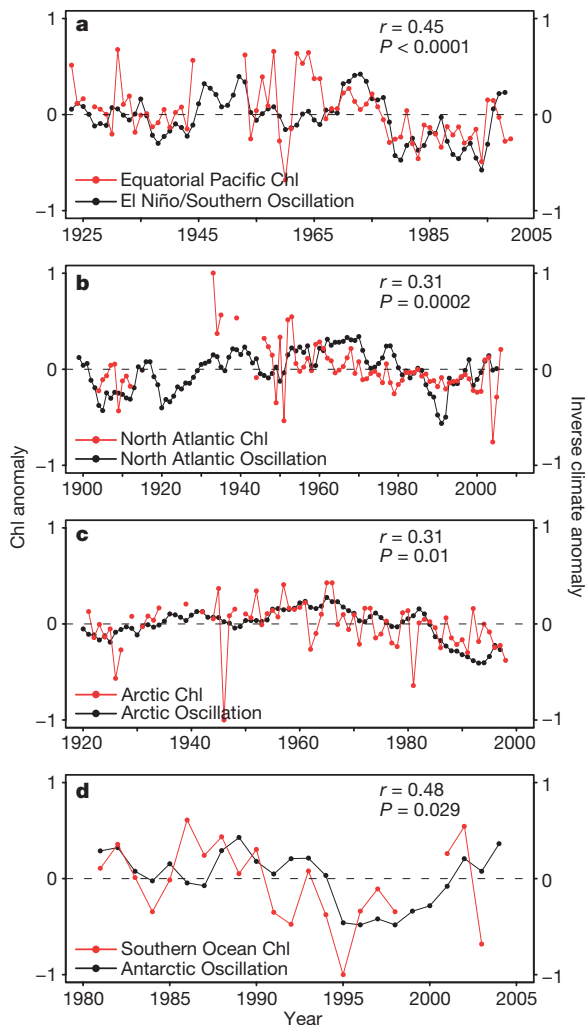


**Figure 5 | Effects of climate variability on phytoplankton.** a–d, Linear relationships between normalized and de-trended yearly Chl anomalies (red) and smoothed climate indices (black) for the Equatorial Pacific (a), the North Atlantic (b), the Arctic (c) and the Southern Ocean (d) regions. Pearson correlation coefficients and  $P$ -values are shown. Climate indices and correlation coefficients have been inverted in order to better visualize correlations.

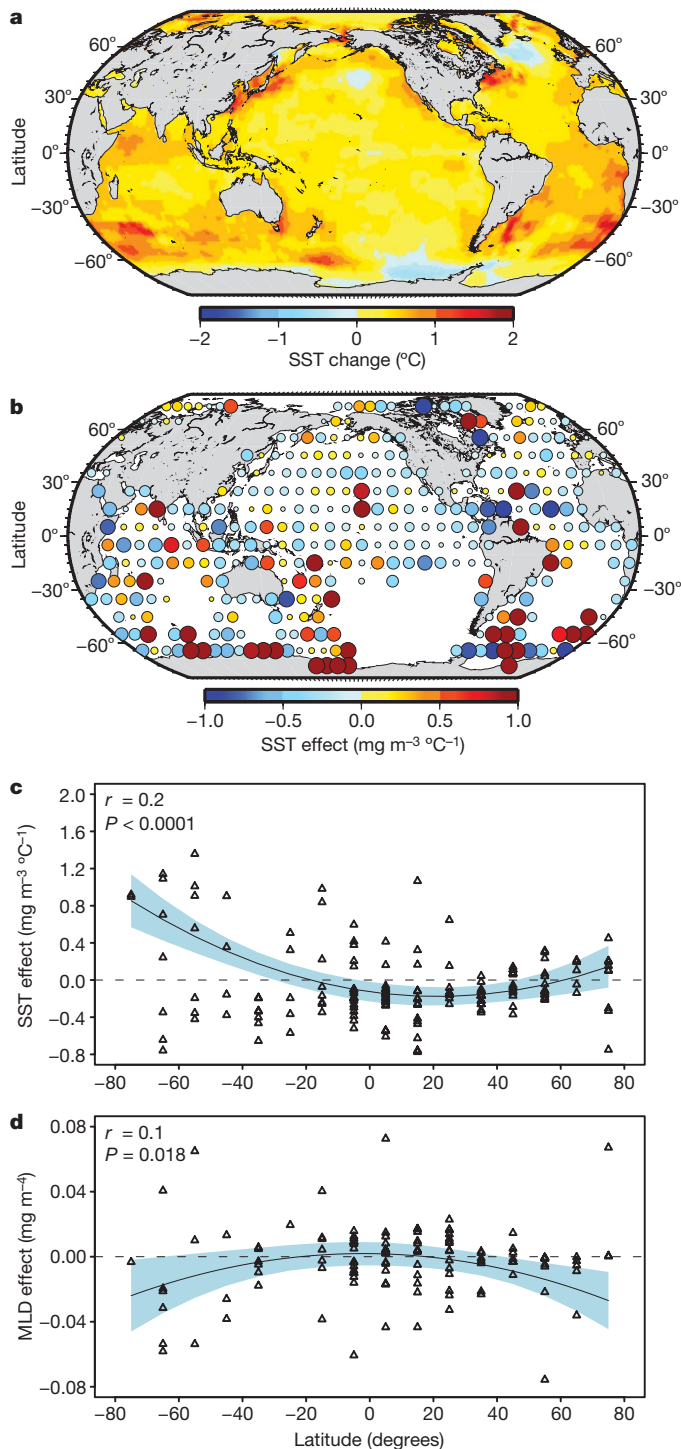


**Figure 6 | Physical drivers of phytoplankton trends.** **a**, Estimated SST change at 1° resolution from 1899 to 2009. Blue represents cells where SST has declined while yellow and red represent increases. **b**, Effects of SST changes on Chl estimated for each 10° × 10° cell with >10 yr of data ( $n = 205$ ). Size of circles represents the magnitude and colours depict the sign of the standardized SST effect on Chl in each cell. **c**, **d**, Effects of SST (**c**) and MLD (**d**) on Chl as a function of latitude (data points). Relationships were best approximated as quadratic functions of latitude (fitted lines and test statistics). Blue shading represents 95% confidence limits.

### Conclusions

Our analysis suggests that global Chl concentration has declined since the beginning of oceanographic measurements in the late 1800s. Multiple lines of evidence suggest that these changes are generally related to climatic and oceanographic variability and particularly to increasing SST over the past century (Fig. 6). The negative

effects of SST on Chl trends are particularly pronounced in tropical and subtropical oceans, where increasing stratification limits nutrient supply. Regional climate variability can induce variation around these long-term trends (Fig. 4), and coastal processes such as land runoff may modify Chl trends in nearshore waters. The long-term global declines observed here are, however, unequivocal. These results provide a larger context for recently observed declines in remotely sensed Chl<sup>7,10,22</sup>, and are consistent with the hypothesis that increasing ocean warming is contributing to a restructuring of marine ecosystems<sup>36,37</sup>, with implications for biogeochemical cycling<sup>15</sup>, fishery yields<sup>38</sup> and ocean circulation<sup>3</sup>. Such consequences provide incentive for an enhanced *in situ* and space-borne observational basis to reduce uncertainties in future projections.

### METHODS SUMMARY

**Data.** Available upper ocean (<20 m) *in situ* Chl data were extracted from the National Oceanographic Data Center (NODC; <http://www.nodc.noaa.gov/>) and the Worldwide Ocean Optics Database (WOOD; <http://wood.jhuapl.edu/wood/>). After removing duplicate observations, mean *in situ* Chl over the upper 20 m was calculated for each cast. Ocean transparency data were extracted from NODC, WOOD, and the Marine Information Research Center (MIRC). Chl (mg m<sup>-3</sup>) was estimated from transparency measurements as

$$\text{Chl} = 457D^{-2.37} \quad (1)$$

where  $D$  is Secchi depth in metres (ref. 17). As data may be affected by sampling and data entry errors, we filtered erroneous or biologically implausible measurements. **Analysis.** Chl trends were estimated for each 10° × 10° cell containing adequate data ('local' models, Fig. 2b) and for each regional area ('regional' models, Fig. 3b). GAMs were fitted to the blended data to estimate Chl trends as follows:

$$\eta(\mu_i) = B_0 + B_1 \text{Year}_i + B_2 \text{Bathymetry}_i + f_2(\text{Latitude}_i, \text{Longitude}_i) + f_3(\text{Day}) + \varepsilon_i \quad (2)$$

where  $\eta$  is the monotonic link function of the expected mean Chl concentration  $\mu_i$ ,  $B_0$  is the model intercept,  $B_i$  and  $f_i$  are respectively parametric and non-parametric effects estimated from the data, and  $\varepsilon_i$  is an error term. A  $\Gamma$ -distributed error structure and a log link were used. The global mean rate of Chl change (Fig. 3b) was estimated by calculating an inverse variance-weighted random-effects meta-analytic mean<sup>39</sup> from the ten regional estimates (see Supplementary Information for full details).

SST changes (Fig. 6a) were estimated by fitting linear models to data in each 1° × 1° cell and area-weighted additive models to data in each of the ten regions. To examine the effects of physical drivers (SST, MLD, wind), Chl and physical data sets were merged by location (1° cell) and time (year, month), and GAMs were fitted with an added effect for the physical driver in question.

Received 21 January; accepted 9 June 2010.

- Field, C. B., Behrenfeld, M. J., Randerson, J. T. & Falkowski, P. Primary production of the biosphere: integrating terrestrial and oceanic components. *Science* **281**, 237–240 (1998).
- Chassot, E. *et al.* Global marine primary production constrains fisheries catches. *Ecol. Lett.* **13**, 495–505 (2010).
- Murtugudde, I., Beauchamp, R. J., McClain, C. R., Lewis, M. R. & Busalacchi, A. Effects of penetrative radiation on the upper tropical ocean circulation. *J. Clim.* **15**, 470–486 (2002).
- Sabine, C. L. *et al.* The oceanic sink for anthropogenic CO<sub>2</sub>. *Science* **305**, 367–371 (2004).
- Roemmich, D. & McGowan, J. Climatic warming and the decline of zooplankton in the California current. *Science* **267**, 1324–1326 (1995).
- McClain, C. R. A decade of satellite ocean color observations. *Annu. Rev. Mar. Sci.* **1**, 19–42 (2009).
- Gregg, W. W. & Conkright, M. E. Decadal changes in global ocean chlorophyll. *Geophys. Res. Lett.* **29**, 1730–1734 (2002).
- Gregg, W. W., Casey, N. W. & McClain, C. R. Recent trends in global ocean chlorophyll. *Geophys. Res. Lett.* **32**, 1–5 (2005).
- Antoine, D., Morel, A., Gordon, H. R., Banzon, V. F. & Evans, R. H. Bridging ocean color observations of the 1980s and 2000s in search of long-term trends. *J. Geophys. Res.* **110**, 1–22 (2005).
- Behrenfeld, M. J. *et al.* Climate-driven trends in contemporary ocean productivity. *Nature* **444**, 752–755 (2006).
- Martinez, E., Antoine, D., D'Ortenzio, F. & Gentili, B. Climate-driven basin-scale decadal oscillations of oceanic phytoplankton. *Science* **326**, 1253–1256 (2009).

12. Falkowski, P. G., Barber, R. T. & Smetacek, V. Biogeochemical controls and feedbacks on ocean primary production. *Science* **281**, 200–206 (1998).
13. Raitsos, D. E., Reid, P. C., Lavender, S. J., Edwards, M. & Richardson, A. J. Extending the SeaWiFS chlorophyll data set back 50 years in the northeast Atlantic. *Geophys. Res. Lett.* **32**, 1–4 (2005).
14. Ryther, J. H. & Yentsch, C. S. The estimation of phytoplankton production in the ocean from chlorophyll and light data. *Limnol. Oceanogr.* **2**, 281–286 (1957).
15. Henson, S. A. *et al.* Detection of anthropogenic climate change in satellite records of ocean chlorophyll and productivity. *Biogeosciences* **7**, 621–640 (2010).
16. Jeffrey, S. W., Mantoura, R. F. C. & Wright, S. W. *Phytoplankton Pigments in Oceanography* Vol. 10 (UNESCO, 1997).
17. Falkowski, P. & Wilson, C. Phytoplankton productivity in the North Pacific ocean since 1900 and implications for absorption of anthropogenic CO<sub>2</sub>. *Nature* **358**, 741–743 (1992).
18. Lewis, M. R., Kuring, N. & Yentsch, C. Global patterns of ocean transparency: implications for the new production of the open ocean. *J. Geophys. Res.* **93**, 6847–6856 (1988).
19. Hastie, T. & Tibshirani, R. Generalized additive models. *Stat. Sci.* **1**, 297–318 (1986).
20. Ware, D. M. & Thomson, R. E. Bottom-up ecosystem trophic dynamics determine fish production in the Northeast Pacific. *Science* **308**, 1280–1284 (2005).
21. Vantrepotte, V. & Melin, F. Temporal variability of 10-year global SeaWiFS time-series of phytoplankton chlorophyll *a* concentration. *ICES J. Mar. Sci.* **66**, 1547–1556 (2009).
22. Polovina, J. J., Howell, E. A. & Abecassis, M. Ocean's least productive waters are expanding. *Geophys. Res. Lett.* **35**, L03618, doi:10.1029/2007GL031745 (2008).
23. Pauly, D. & Christensen, V. Primary production required to sustain global fisheries. *Nature* **374**, 255–257 (1995).
24. Behrenfeld, M. J., Boss, E., Siegel, D. A. & Shea, D. M. Carbon-based ocean productivity and phytoplankton physiology from space. *Glob. Biogeochem. Cycles* **19**, 1–14 (2005).
25. Yoder, J. A. & Kennelly, M. A. Seasonal and ENSO variability in global ocean phytoplankton chlorophyll derived from 4 years of SeaWiFS measurements. *Glob. Biogeochem. Cycles* **17**, 1–24 (2003).
26. Behrenfeld, M. J. *et al.* Biospheric primary production during an ENSO transition. *Science* **291**, 2594–2597 (2001).
27. Wiggert, J. D., Murtugudde, R. G. & Christian, J. R. Annual ecosystem variability in the tropical Indian Ocean: results of a coupled bio-physical ocean general circulation model. *Deep Sea Res. II* **53**, 644–676 (2006).
28. Mann, K. H. & Lazier, J. R. N. *Dynamics of Marine Ecosystems* (Blackwell, 1991).
29. Dickson, R. R., Kelly, P. M., Colebrook, J. M., Wooster, W. S. & Cushing, D. H. North winds and production in the production in the eastern North Atlantic. *J. Plankton Res.* **10**, 151–169 (1988).
30. Fromentin, J. M. & Planque, B. *Calanus* and environment in the eastern North Atlantic. 2. Influence of the North Atlantic Oscillation on *C. finmarchicus* and *C. helgolandicus*. *Mar. Ecol. Prog. Ser.* **134**, 111–118 (1996).
31. Paytan, A. *et al.* Toxicity of atmospheric aerosols on marine phytoplankton. *Proc. Natl Acad. Sci. USA* **10**, 4601–4605 (2009).
32. Montes-Hugo, M. *et al.* Recent changes in phytoplankton communities associated with rapid regional climate change along the western Antarctic peninsula. *Science* **323**, 1470–1473 (2009).
33. Broecker, W. S., Sutherland, S. & Peng, T.-H. A possible 20th century slowdown of Southern Ocean deep water formation. *Science* **286**, 1132–1134 (1999).
34. Frank, K. T., Petrie, B., Choi, J. S. & Leggett, W. C. Trophic cascades in a formerly cod-dominated ecosystem. *Science* **308**, 1621–1623 (2005).
35. Doney, S. C. Plankton in a warmer world. *Nature* **444**, 695–696 (2006).
36. Richardson, A. J. & Schoeman, D. S. Climate impact on plankton ecosystems in the Northeast Atlantic. *Science* **305**, 1609–1612 (2004).
37. Worm, B. & Lotze, H. K. in *Climate and Global Change: Observed Impacts on Planet Earth* (ed. Letcher, T.) 263–279 (Elsevier, 2009).
38. Brander, K. M. Global fish production and climate change. *Proc. Natl Acad. Sci. USA* **104**, 19709–19714 (2007).
39. Cooper, H. & Hedges, L. V. *The Handbook of Research Synthesis* (Russell Sage Foundation, 1994).

**Supplementary Information** is linked to the online version of the paper at [www.nature.com/nature](http://www.nature.com/nature).

**Acknowledgements** We are grateful to all data providers, to J. Mills-Flemming, W. Blanchard, M. Dowd, C. Field and C. Minto for statistical advice, to T. Boyer, J. Smart, D. Ricard and D. Tittensor for help with data extraction, and to J. Mills-Flemming, W. Blanchard, W. Li, H. Lotze, C. Muir and M. Dowd for critical review. Funding was provided by the Natural Sciences and Engineering Research Council of Canada, the US Office of Naval Research, the Canada Foundation for Climate and Atmospheric Sciences, the National Aeronautics and Space Administration, the Sloan Foundation (Census of Marine Life FMAP Program), and the Lenfest Ocean Program.

**Author Contributions** The study was initiated by B.W. and M.R.L. in collaboration with the late R.A. Myers. Data were compiled by D.G.B. and M.R.L.; D.G.B. conducted the analyses and drafted the manuscript. All authors discussed the results and contributed to the writing of the manuscript.

**Author Information** Reprints and permissions information is available at [www.nature.com/reprints](http://www.nature.com/reprints). The authors declare no competing financial interests. Readers are welcome to comment on the online version of this article at [www.nature.com/nature](http://www.nature.com/nature). Correspondence and requests for materials should be addressed to D.G.B. ([dboyce@dal.ca](mailto:dboyce@dal.ca)).